Physics

Physics Research Publications

Purdue University   *Year* 2005

Warm-hot gas in and around the Milky Way: Detection and implications of OVII absorption toward LMC X-3

Q. D. Wang, Y. Yao, T. M. Tripp, T. T. Fang, W. Cui, F. Nicastro, S. Mathur,
R. J. Williams, L. Song, and R. Croft

WARM-HOT GAS IN AND AROUND THE MILKY WAY: DETECTION AND IMPLICATIONS OF O VII ABSORPTION TOWARD LMC X-3

Q. D. WANG,[1] Y. YAO,[1] T. M. TRIPP,[1] T.-T. FANG,[2] W. CUI,[3] F. NICASTRO,[4]
S. MATHUR,[5] R. J. WILLIAMS,[5] L. SONG,[1] AND R. CROFT[6]

ABSTRACT

X-ray absorption lines of highly ionized species such as O VII at about zero redshift have been firmly detected in the spectra of several active galactic nuclei. However, the location of the absorbing gas remains a subject of debate. To separate the Galactic and extragalactic contributions to the absorption, we have obtained *Chandra* LETG-HRC and *Far Ultraviolet Spectroscopic Explorer* observations of the black hole X-ray binary LMC X-3. We clearly detect the O VII Kα absorption line with an equivalent width of 20(14, 26) mÅ (90% confidence range). The Ne IX Kα absorption line is also detected, albeit marginally. A joint analysis of these lines, together with the nondetection of the O VII Kβ and O VIII Kα lines, gives the temperature, velocity dispersion, and hot oxygen column density as $1.3(0.7, 1.8) \times 10^6$ K, 79(62,132) km s^{-1}, and 1.9(1.2, 3.2) $\times 10^{16}$ cm^{-2}, assuming a collisional ionization equilibrium of the X-ray-absorbing gas and a Galactic interstellar Ne/O number ratio of 0.18. The X-ray data allow us to place a 95% confidence lower limit to the Ne/O ratio as 0.14, but the upper limit is not meaningfully constrained. The O VII line centroid and its relative shift from the Galactic O I Kα absorption line, detected in the same observations, are *inconsistent* with the systemic velocity of LMC X-3 (+310 km s^{-1}). The far-UV spectrum shows O VI absorption at Galactic velocities, but no O VI absorption is detected at the LMC velocity at greater than 3 σ significance. The measured Galactic O VI column density is higher than the value predicted from the O VII-bearing gas, indicating multiphase absorption. Both the nonthermal broadening and the decreasing scale height with the increasing ionization state further suggest an origin of the highly ionized gas in a supernova-driven galactic fountain. In addition, we estimate the warm and hot electron column densities from our detected O II Kα line in the LMC X-3 X-ray spectra and from the dispersion measure of a pulsar in the LMC vicinity. We then infer the O/H ratio of the gas to be $\gtrsim 8 \times 10^{-5}$, consistent with the chemically enriched galactic fountain scenario. We conclude that the Galactic hot interstellar medium should in general substantially contribute to zero-redshift X-ray absorption lines in extragalactic sources.

Subject headings: intergalactic medium — ISM: kinematics and dynamics — stars: individual (LMC X-3) — techniques: spectroscopic — ultraviolet: ISM — X-rays: ISM

1. INTRODUCTION

Recently, several groups have reported the detection of H- and He-like oxygen absorption lines from the local ($cz \sim 0$) hot gas in the X-ray spectra of active galactic nuclei (AGNs) with the *Chandra X-Ray Observatory* and *XMM-Newton* (Fang et al. 2002b, 2003; Nicastro et al. 2002; Rasmussen et al. 2003; McKernan et al. 2004; Williams et al. 2005). The detected column densities of highly ionized oxygen are around 10^{16} cm^{-2}, which has been suggested to be an indication of the presence of large amounts of intergalactic "warm-hot" gas at temperatures around $\sim 10^6$ K. This suggestion, if confirmed, would have strong implications for our understanding of the so-called missing baryon problem (Fukugita et al. 1998; Cen & Ostriker 1999; Davé et al. 2001; Fang et al. 2002a; Nicastro et al. 2005). In turn, by comparing nearby X-ray absorbers to highly UV ionized absorption systems observed at various redshifts from $z \approx 0.2$ out to $z \gtrsim 4$ (Tripp et al. 2000; Reimers et al. 2001; Simcoe et al. 2002; Kirkman & Tytler 1997), these data could shed light on the thermal and chemical evolution of the universe. However, one critical question remains open: where are these highly ionized $cz \sim 0$ X-ray

absorbers—in the interstellar medium (ISM) of the Galactic disk, in an extended Galactic halo, in the Local Group, or even beyond?

We here report *Chandra* grating observations of LMC X-3 in its high state to discriminate between the Galactic and extragalactic scenarios of the O VII absorption. Because this bright X-ray source is in our neighboring galaxy, the Large Magellanic Cloud (LMC), at the distance of ~ 50 kpc, the detection of the absorption offers a direct measurement of the hot gas content along a line of sight through essentially the entire Galaxy, including its halo. The consistency between this measurement and those in the AGN sight lines provides a direct constraint on the residual absorption on scales greater than the LMC distance. We supplement the *Chandra* data with a nearly simultaneous far-UV observation obtained with the *Far Ultraviolet Spectroscopic Explorer* (*FUSE*).

LMC X-3 is perhaps the best-suited source for this experiment. Among the several bright X-ray binaries in both the Small and Large Magellanic Clouds, LMC X-3 normally exhibits a very soft X-ray spectrum, which is dominated by the accretion disk emission, and an exceptionally high luminosity during its high state. Unlike most black hole systems, LMC X-3 spends most of its time in the high state. LMC X-3 is outside the main body of the LMC and is about 5° away from the active star-forming 30 Doradus region, where LMC X-1 and two neutron star X-ray binaries (X-2 and X-4) are located (Fig. 1). Therefore, the potential absorption contribution from hot gas local to the LMC is minimal. Finally, LMC X-3 has a systemic velocity of $+310 \pm 7$ km s^{-1}, comparable to the expected velocity ($+343$ km s^{-1}) for

[1] Astronomy Department, University of Massachusetts, Amherst, MA 01003; wqd@astro.umass.edu, yaoys@astro.umass.edu.
[2] Astronomy Department, University of California, Berkeley, CA.
[3] Physics Department, Purdue University.
[4] Harvard-Smithsonian Center for Astrophysics.
[5] Department of Astronomy, The Ohio State University, Columbus, OH.
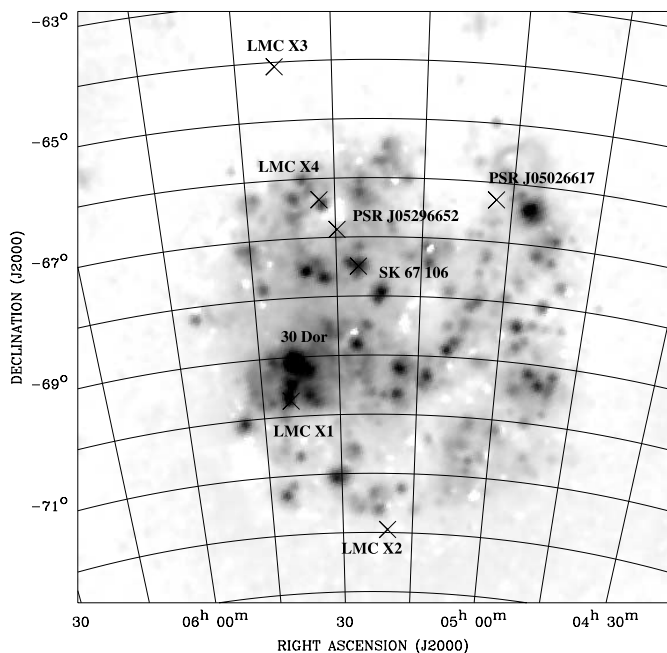[6] Physics Department, Carnegie Mellon University.

FIG. 1.—Hα image of the LMC (Finkbeiner 2003) with the marked locations of several objects mentioned in the text.

FIG. 2.—*RXTE* ASM (1.5–12 keV) count rate of LMC X-3 plotted vs. Julian date. The short dashed bars mark the *Chandra* observation dates.

the projected location in the LMC (Cowley et al. 1983). This velocity makes it relatively straightforward to distinguish a spectral line that is local to the X-ray binary or to the LMC from that associated with the Galactic disk.

We have analyzed and interpreted the *Chandra* and *FUSE* data almost independently, but the results and conclusions found are in nearly complete agreement. Therefore, we try to keep this independence in the presentation of this paper. We adopt the Galactic ISM metal abundances given by Wilms et al. (2000) (e.g., the oxygen and neon number fractions are 4.90×10^{-4} and 8.71×10^{-5}, compared to the typically assumed solar values 6.76×10^{-4} and 1.20×10^{-4}; Grevesse & Sauval 1998); both the constraint on the abundances and the effect of the relative elemental fraction change on our results are discussed in § 4. Furthermore, our spectroscopic analysis assumes that the X-ray-absorbing gas is in a collisional ionization equilibrium (CIE). The parameter uncertainties in this paper are quoted at the 68% and 90% confidence levels for the far-UV and X-ray measurements, respectively, unless otherwise noted.

2. OBSERVATIONS AND DATA REDUCTION

2.1. *Chandra Observations*

Our experiment used the *Chandra* low energy transmission grating plus the high resolution camera (LETG-HRC) combination, chiefly for its high sensitivity to detect the O VII Kα line. The spectral resolution of the LETG-HRC is 0.05 Å (FWHM). LMC X-3 is a variable black hole X-ray binary and its soft X-ray flux varies quasi-periodically on a period of 99 or 199 days (Cowley et al. 1991; Cowley et al. 1983). We thus proposed the experiment as a target of opportunity (ToO) program during the *Chandra* cycle 5. Because of the newly imposed solar pitch angle constraints on *Chandra* pointing duration, our proposed 100 ks exposure was split into three separate observations of 20, 40, and 40 ks, taken on 2004 April 20, May 4, and May 8 (Fig. 2). Unfortunately, the X-ray intensity of LMC X-3 decreased unusually rapidly from the peak when the ToO was triggered; by the time of the latter two (longer) observations, the count rates had dropped
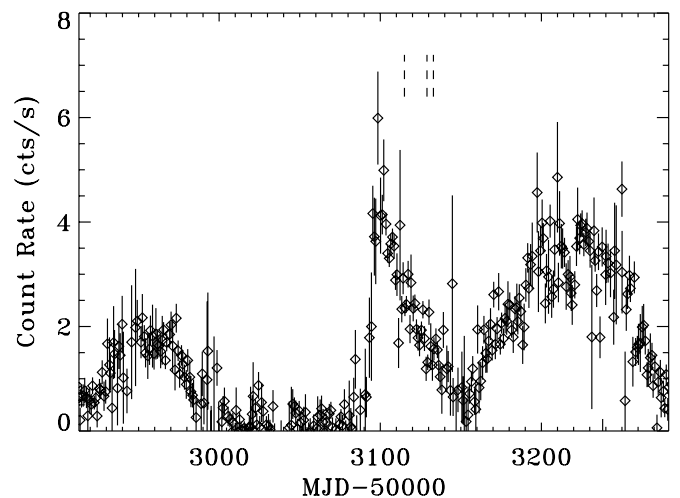
by a factor of ~2. Nevertheless, we still collected more than 4×10^5 good events in the energy range 10–40 Å along the two high-resolution grating arms.

We processed the LMC X-3 data, using the standard CIAO threads (ver. 3.2.1)[7] with the calibration database CALDB (ver. 3.0.0).[8] As described in the Observatory Guide (ver. 7.0),[9] "the LETG diffracts X-rays into a dispersed spectrum according to the grating diffraction relation, $m\lambda = p \sin \theta$, where m is the integer order number, λ the photon wavelength, p the spatial period of the grating lines, and θ the dispersion angle." Therefore, events recorded at each θ of an observation consist of photons at multiple wavelengths in different orders. Generally, this spectral order overlapping is most serious at long wavelengths, because both the intrinsic source photon flux and the effective collecting area of the telescope/instrument decrease with photon energy. The overlapping orders cannot be sorted out locally in an observed spectrum, because the HRC itself lacks sufficient energy resolution.

We used a forward modeling approach to globally account for the spectral order overlapping (§ 3.1). To facilitate such modeling, we constructed a grating response matrix file (RMF) and an auxiliary response (or effective area) function (ARF) for each order (from the first to the sixth) of each grating arm, by running the threads `mkgrmf` and `mkgarf`. We then added the six ARF and RMF pairs together to form an order-combined response file (RSP)[10] for each grating arm. This RSP file accounts for not only the local line response, but also the global spectral overlapping of the orders. For ease of processing and visualization, we further co-added the spectra: first the negative and positive arms, and then the individual observations. The corresponding RSP files were averaged channel by channel and weighted by the best-fit global models of individual spectra (see § 3.1). As a consistency check, our analysis was often repeated with the individual spectra before the co-adding.

2.2. *FUSE Observations*

To complement the *Chandra* observations, we also obtained high-resolution ultraviolet spectroscopy of LMC X-3 via a ToO

---

observation with *FUSE*.[11] The *FUSE* data cover the O vi res-onance-line doublet at 1031.93 and 1037.62 Å, which is valu-able for understanding the ionization and single phase versus multiphase nature of highly ionized absorbers (Tripp & Savage 2000; Tripp et al. 2001; Mathur et al. 2003; Sembach et al. 2004, Savage et al. 2005a, 2005b; Collins et al. 2005). More-over, the spectral resolution of *FUSE* (FWHM $\approx$ 20 km s^{-1}) is at least an order of magnitude higher than that of any current X-ray spectrograph. Consequently, the *FUSE* observation pro-vides robust information about the kinematics and line broad-ening as well as the likely location of the gas (the Milky Way vs. the LMC) based on line velocities. In CIE, the population of O vi ions peaks sharply at $\sim 10^{5.5}$ K, whereas O vii and Ne ix trace gas over a broad temperature range ($10^{5.5}$–$10^{6.5}$ K; Yao & Wang 2005). However, in terms of column density detection, the *FUSE* ob-servation is more sensitive to O vi than the *Chandra* observation is to O vii and can actually be used to trace gas with a temperature as high as $\sim 10^6$ K.

The *FUSE* and *Chandra* observations were coordinated to occur as simultaneously as possible. The requirement of simulta-neous X-ray and UV observations was primarily for investigation of the accretion disk physics and intrinsic properties of LMC X-3, which will be presented in a separate paper. The *FUSE* data were obtained in a single visit on 2004 April 20 for a total on-source integration time of 88.9 ks. The program employed the LWRS ($30'' \times 30''$) aperture and time-tag mode, but only data from the LiF1 channel were useful (other channels were not adequately co-aligned). The data were reduced with CALFUSE (ver. 3.0.7) following standard procedures.[12] For *FUSE*, LMC X-3 is a rela-tively faint target, and it is difficult to determine shifts between subexposures for alignment and co-addition. However, since all subexposures were obtained during a single visit, such shifts should be small or negligible in the LiF1 channel. The final, co-added spectrum was binned to ~ 7.5 km s^{-1} pixels (roughly 3 pix-els per resolution element).

Before execution of our program, LMC X-3 had been ob-served with *FUSE* in 2002 (see Hutchings et al. 2003). While the total integration time (~ 24 ks) obtained by Hutchings et al. was significantly shorter than the exposure time of the new observa-tion, it turns out that LMC X-3 was also substantially brighter (in the UV region near the O vi doublet) when Hutchings et al. ob-served it. Consequently, the signal-to-noise ratios of the old and new observations are comparable. In principle, if some absorp-tion is circumstellar, then the absorption lines could vary between observations. However, we have acquired and re-reduced the older LMC X-3 *FUSE* data obtained by Hutchings et al., and we find that the absorption lines in the old and new data appear to be identical within the noise. Therefore, we have elected to co-add all of the data (LiF1a and LiF2b from Hutchings et al. and LiF1a from the new program). Because the flux varied significantly be-tween the 2002 and 2004 observations, we fitted the continua of the three spectra independently and then coadded the continuum-normalized data, weighted inversely by their variances. The con-tinua were fitted with low-order polynomials in the regions within ± 1000 km s^{-1} of the O vi $\lambda 1031.93$ line.

Hutchings et al. (2003) found that the velocity of the O vi emission centroid varies by 100–150 km s^{-1} as a function of the X-ray binary phase, and they derived an orbital semiamplitude of 130–200 km s^{-1} for the putative black hole in LMC X-3. Our new observations show a narrow O vi emission feature at LMC

velocities that shifts position as the binary phase changes, and the shifts are in the same direction as reported by Hutchings et al. However, the shifting O vi emission feature in the new data is nar-rower than the emission presented by Hutchings et al. We will present a full analysis of the O vi emission in a separate paper. However, it is relevant here because the narrow O vi emission can lead to a complicated continuum shape against which absorption is measured. Misplacement of the continuum due to the emission could cause absorption features to be incorrectly measured. To avoid this problem, before co-adding the data, we collected the data into five phase ranges. In each phase range, we examined the spectrum to identify the wavelength range affected by the narrow O vi emission, and we masked and excluded that wavelength range from the final, co-added spectrum. Because the O vi emission is narrow and shifts substantially in velocity, this masking procedure still allowed accumulation of adequate signal at all wavelengths, i.e., no regions of the spectrum were masked out entirely.

3. ANALYSIS AND RESULTS

3.1. *Chandra Data*

Our *Chandra* spectral analysis uses the software XSPEC (ver-sion 11.3.1). To properly account for the spectral order over-lapping (§ 2.1), we model the entire observed spectrum in the 2–41 Å range. We first try an absorbed disk blackbody plus power law model, but obtain a poor spectral fit (χ^2/dof = 3980/3114, cor-responding to a statistical null hypothesis confidence of $\sim 3 \times 10^{-24}$). This poor fit is largely due to various local deviations from the model. These deviations are likely due to the current imperfect calibration of the instrument response (i.e., the adopted RSP), which does not accurately account for such effects as the dithered HRC-S plate gaps (Nicastro et al. 2005), and to the uncertainties in various emission and absorption models (e.g., neutral absorp-tion edges; Juett et al. 2004). Following Nicastro et al. (2005), we include eight broad Gaussian components (three positive and five negative) to account for such local spectral deviations. The inclusion of these broad components improves the continuum fit substantially (χ^2/dof = 3308/3090) and typically has insignifi-cant effects on narrow lines that we want to measure. We find that the O i, O ii,[13] Ne ix and O vii Kα absorption lines are clearly vis-ible at their expected rest-frame wavelengths (Fig. 3; the rele-vant atomic parameters and references are summarized in Table 3 of Yao & Wang 2005). These lines are characterized with four negative Gaussian profiles (each reducing the degrees of free-dom by three), which further improve the spectral fit (reducing χ^2 consecutively by 80, 24, 16, and 35). The final best fit is rea-sonably acceptable (χ^2/dof = 3153/3078) and is shown in Fig-ure 4. The order overlapping is considerable in the wavelength range longward of 10 Å. The contribution from orders higher than the first is $\sim 7\%$, 30%, 50%, and 75% at wavelength 13, 21, 33, and 40 Å respectively. Accounting for the contamination from orders higher than the first one, we estimate the equivalent widths (EWs) and centroid velocities (relative to the rest frame) of the lines as presented in Table 1. We also obtain the one-sided 95% confidence upper bounds to the EWs of O vii Kβ and O viii Kα absorption lines (listed in Table 1), by fixing their centroids to the rest-frame energies and jointly fitting their line widths with the O vii Kα line. The inclusion of these two line components in the fit does not significantly reduce the χ^2/dof (= 3150/3076). We further check the centroid and EW of the O vii Kα line in the
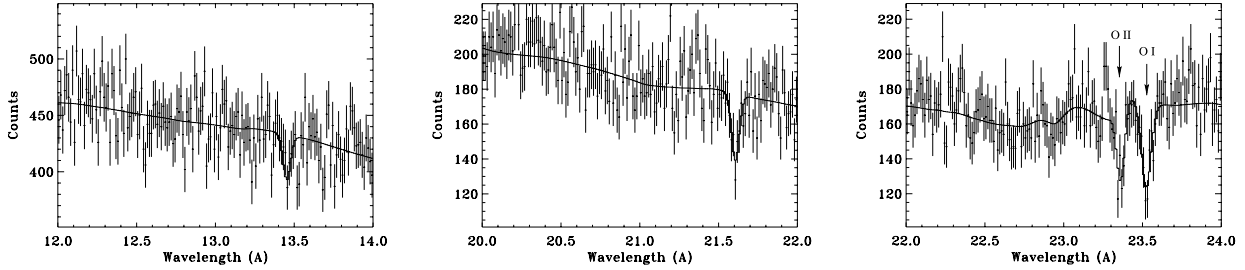

FIG. 3.—Close-ups of the *Chandra* LETG-HRC spectrum of LMC X-3 around the Kα lines of (*left*) Ne IX , (*middle*) O VII , and (*right*) O I and O II. In each panel, the curves represent the fitted continuum plus a negative *Gaussian* line model, which has been convolved with the RSP. The bin size is 0.0125 Å.

three observations separately, and we find no evidence for any significant variation.

To estimate the physical parameters of the X-ray-absorbing gas, we jointly fit the O VII Kα, O VII Kβ, O VIII Kα, and Ne IX Kα lines, using the multiplicative absorption line model, `absline`, as detailed in Yao & Wang (2005). Briefly, the model adopts an accurate absorption line profile (Voigt function) and accounts for the line saturation automatically. This `absline` fit with three free parameters fewer than in the above Gaussian line fit, has a similar quality ($\chi^2/$dof $= 3152/3079$). The best-fit model is shown in Figure 5. The fitted parameters are the absorbing gas temperature $\log [T(\mathrm{K})] = 6.1(5.9, 6.3)$, the velocity dispersion $b_v = 79(62, 132)$ km s^{-1}, and the equivalent hydrogen column density $\log N_{\mathrm{H}}(\mathrm{cm}^{-2})] = 19.6(19.4, 19.8)$ with a corresponding $\log N_{\mathrm{O\,VII}}(\mathrm{cm}^{-2})] = 16.3(16.1, 16.5)$. Figure 6 shows $N_{\mathrm{H}} - b_v$ confidence contours. The fitted line centroid velocities are nearly identical to those in Table 1. We can further infer the nonthermal broadening ξ from the definition of $b_v^2 = \xi^2 + 2kT/m_i$, assuming the nonthermal motions are adequately described by a Gaussian profile. Here m_i is the ion mass; so for oxygen, the thermal velocity dispersion is $(2kT/m_i)^{1/2} = 36(29, 47)$ km s^{-1}. Therefore, we infer the nonthermal broadening as $\xi = 70(50, 130)$ km s^{-1}. The `absline` model fitting also allows us to predict l $\log [N_{\mathrm{O\,VI}}(\mathrm{cm}^{-2})] = 13.8(13.6, 14.3)$.

Because our joint fit of the absorption lines utilizes all the information available in the spectrum, the source of a particular parameter constraint cannot be isolated easily. But fundamentally, from our measurements we have both lower and upper bounds on the O VII and Ne IX Kα absorption lines and only upper bounds on the O VII Kβ and O VIII Kα lines, i.e., a total of six measurements. Thus we can, in principle, solve for six limits on the parameters: T, b_v, $N_{\mathrm{O\,VII}}$, and $N_{\mathrm{Ne\,IX}}$, or their combinations. With the assumption of the Galactic ISM Ne/O ratio, we can then constrain all the parameters. In fact, we can do a bit better, considering that T and b_v are not totally independent and that the demand for the very existence of the solution places additional constraint on the parameters, as is demonstrated in the following discussion.

We can better illustrate how the specific parameter constraints may be realized by using an alternative (but not independent) approach, the curve-of-growth (CoG) analysis, which is relatively simple and is particularly good for visualization (e.g., Williams et al. 2005). Figure 7 illustrates how N_{H} and b_v can be constrained this way. For an absorption line, its EW, as measured with a negative Gaussian model, is a function of b_v and N_{H}, which is linked to the ionic column density if both element abundance and plasma temperature are assumed. Therefore, from a measured EW and its uncertainties, a region can be constrained in the $N_{\mathrm{H}}-b_v$ plot. With multiple absorption lines from the different transitions of the same ion (e.g., O VII Kα, Kβ, etc.), one may constrain both N_{H} and b_v from the overlapping of the regions. Figure 7 illustrates that the tight constraints on both N_{H} and b_v in our case are derived chiefly from the upper and lower bounds to the O VII Kα,
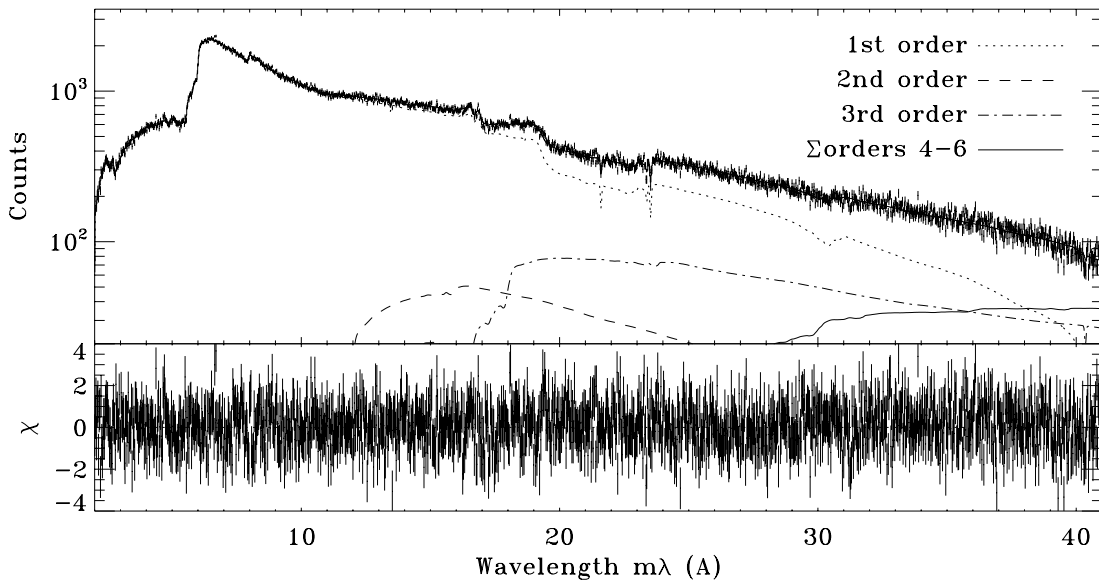

FIG. 4.—Co-added LETG-HRC spectrum of LMC X-3 (*data points with error bars*) and the best-fit continuum model (*solid curve*) and the residuals (*lower panel*). While the fit is based on the original bin size 0.0125 Å, this plotted spectrum has been grouped by a factor of 2 for clarity. Contributions from individual orders are also plotted.

Line	Wavelength (Å)	v (km s^{-1})	EW (mÅ)
O VI	1031.926	55 ± 11	235.8 ± 37.5
O VII Kα	21.6020	56(−83, 194)	20(14, 26)
O VII Kβ...............	18.6270	(fixed)	<7.5
O VIII Kα	18.9670	(fixed)	<4.1
Ne IX Kα..............	13.4470	112(−214, 347)	6.3(3.7, 9.0)
O I Kα	23.5140	128(13, 242)	30(23, 38)
O II Kα	23.3492	283(11, 349)	19(12, 26)

NOTE.—The errors of O VI measurement are at 1 σ levels. The rest-frame wavelengths of O I Kα and O II Kα are taken from the averaged value in Table 2 and Kawatsura et al. (2002), respectively.

the lower bound to Ne IX Kα, and the upper bound to the O VII Kβ EW measurements. Apparently, these four EW bounds do not necessarily lead to a nonzero overlapping region, depending on the assumed T and Ne/O ratio. Therefore, the four EW bounds give constraints not only on both N_H and b_v, but also on the combination of the temperature and abundance, although indirectly. Of course, the upper bounds to O VII Kβ and Ne IX Kα provide additional constraints, especially on the upper limit to T. This apparent overconstraining power of the EW measurements arises from the demand for the existence of a solution (an overlapping region in a multidimensional parameter space).

The CoG approach, however, has its drawbacks. First, it does not use all the information in the spectrum, at least not in a coher-
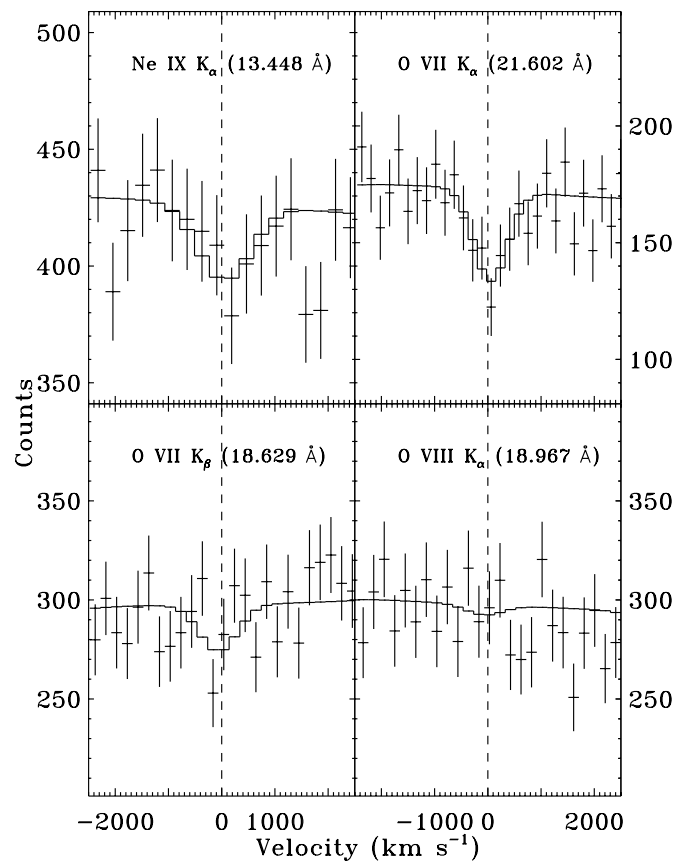

FIG. 6.—Plot of the N_H–b_v confidence contours at 68% and 90% confidence levels constrained in the joint fit with the `absline` model.

ent fashion; absorption lines are measured independently (thus the improved counting statistics from a combination of multiple weak lines is not capitalized). Second, the joint analysis of two or more lines in a CoG diagnostic plot, though informative, does not allow for a rigorous error propagation of the parameter constraints; for example, it is difficult to quantify the overlapping significance and/or to include the uncertainties in the assumed temperature (Fig. 7). Third, the EW measurement from the negative Gaussian model can be problematic, especially when the absorption line is saturated (e.g., an optical depth ∼5 at the line center of the O VII Kα line in the spectrum of LMC X-3); the EW value can be significantly overestimated (see Fig. 4 in Yao & Wang 2005). In fact, a plot like Figure 7 represents only a cut in a multiple dimensional parameter space constrained by the absorption line measurements (e.g., via an `absline` model fit). Therefore, we use the CoG approach only for the visualization and consistency check of the absorption line measurements.

3.2. FUSE Data

We analyzed the FUSE observation entirely independently from the Chandra results, i.e., no constraints from the X-ray data

FIG. 5.—Jointly fitted neon and oxygen absorption lines. The solid histograms represent the best fit from the `absline` + continuum model. The adopted rest-frame energies (Table 1) are marked in each panel. A negative velocity represents a blueshift.
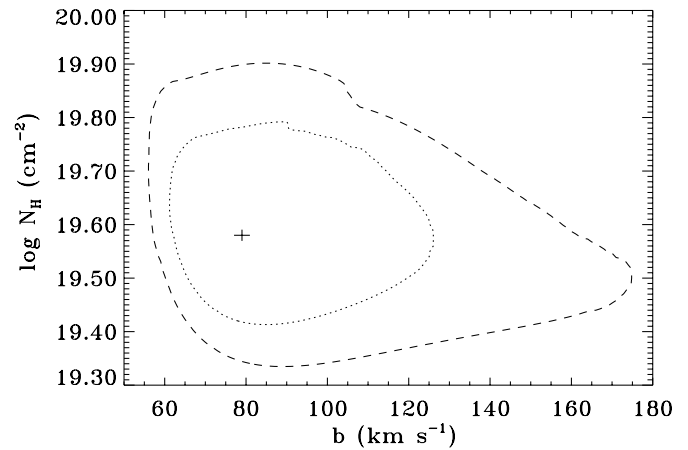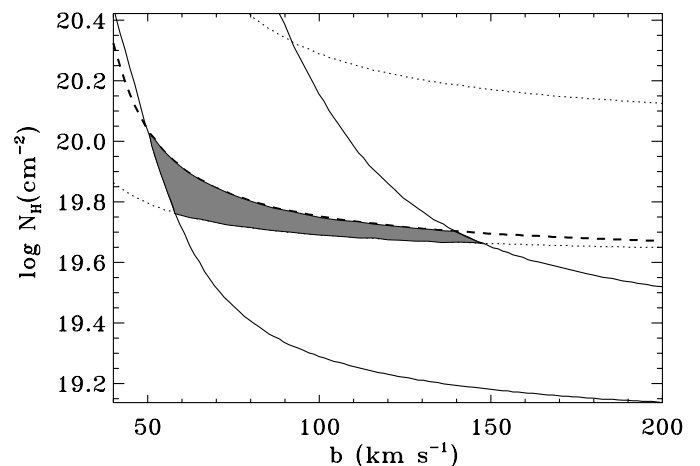

FIG. 7.—Plot of the N_H–b_v diagnostic curves derived from the CoG analysis of the O VII Kα (solid curves), Kβ (thick dashed curve, upper bound only), and Ne IX Kα (dotted curve) absorption lines. These curves enclose the 90% (or 95% one-sided) confidence regions, assuming a CIE hot plasma with a temperature $T = 1.3 \times 10^6$ K. The overlapping region is shaded. This simplistic plot is for illustration purpose only; the actual measurements of the parameters are based on the joint fits of the multiple absorption lines, as detailed in the text.
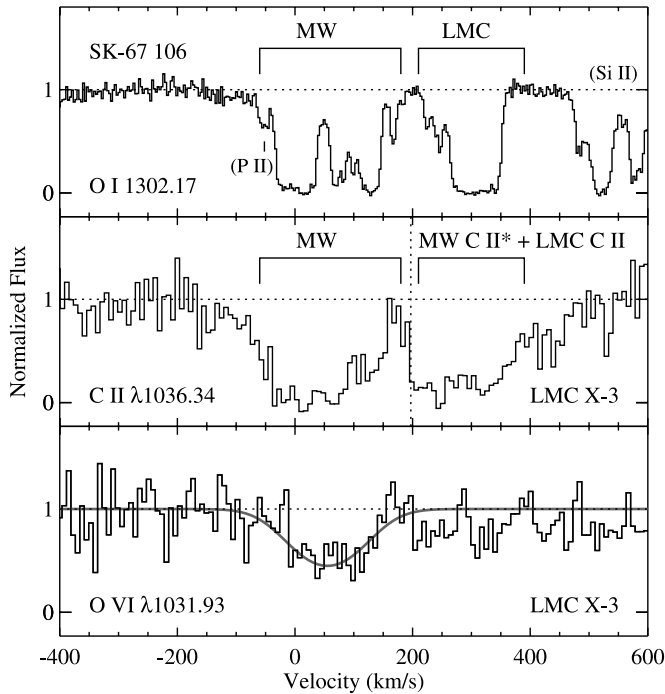
FIG. 8.—Continuum-normalized UV absorption line profiles recorded in the spectrum of LMC X-3, including C II $\lambda1036.34$ (*middle*) and O VI $\lambda1031.93$ (*bottom*), plotted vs. heliocentric velocity. For comparison, the O I $\lambda1302.17$ observed with the STIS E140M echelle toward the B star Sk -67 106 in the LMC is plotted in the top panel. The vertical dotted line in the middle panel indicates the location of C II* $\lambda1037.02$ absorption at $v = 0$ km s^{-1}. A P II line is present near the O I absorption as indicated, but this very weak transition only affects the profile at the marked velocity. The strong Si II $\lambda1304.37$ line is present at $v > 450$ km s^{-1} in the top panel, but this does not affect the O I absorption at $v < 400$ km s^{-1}. Note that the regions used for continuum fitting extend beyond the velocity limits of this plot.

were imposed on the *FUSE* measurements. The low UV flux level makes LMC X-3 a challenging target for *FUSE*, and most of the useful information in the *FUSE* spectrum is in the 1030–1040 Å range where the flux is elevated by a broad emission feature (Hutchings et al. 2003). The middle and lower panels in Figure 8 show the interstellar C II $\lambda1036.34$ and O VI $\lambda1031.93$ lines recorded in the co-added *FUSE* LMC X-3 spectrum. For purposes of comparison, we also show in the upper panel in Figure 8 the interstellar O I $\lambda1302.18$ absorption observed with the Space Telescope Imaging Spectrograph (STIS) toward Sk -67 106, a hot star located in the main body of the LMC (see Fig. 1).[14]

The Sk -67 106 panel in Figure 8 shows that in the general direction of the LMC, strong and complex Milky Way absorption is detected at $0 \lesssim v \lesssim 200$ km s^{-1}, and strong (saturated) absorption due to the ISM of the LMC is present at $200 \lesssim v \lesssim 400$ km s^{-1}. Toward stars located in the main body of the LMC, strong O VI absorption is frequently detected within these velocity ranges as well (e.g., Howk et al. 2002; Danforth et al. 2002). Toward LMC X-3, C II and O VI absorption lines are clearly detected in the Milky Way velocity range. While a strong absorption feature is

evident in the LMC X-3 spectrum at the velocity expected for C II in the LMC ISM, much of that absorption is likely due to a blend of C II* $\lambda1037.02$ and O VI $\lambda1037.62$ from the Milky Way, and it is difficult to reliably assess the amount of LMC C II (or even if it is present at all) in the direction of LMC X-3.

We have measured the equivalent width and column density of the O VI $\lambda1031.93$ absorption by direct integration using the techniques of Sembach & Savage (1992), including assessment of the continuum placement uncertainty as well as statistical uncertainty in the overall error bars. From inspection of Figure 8, we see that O VI absorption is clearly detected at Milky Way velocities ($v \lesssim 200$ km s^{-1}). The O VI EW integrated over the Milky Way velocity range is listed in Table 1; the EW indicates that the Galactic O VI absorption is detected at 6.3 σ significance. The O VI absorption at LMC velocities is much weaker, and integrating over the LMC velocity range (190–390 km s^{-1}), we obtain EW(LMC) = 96.2 ± 46.4 mÅ, i.e., only a 2.1 σ feature. Moreover, if we compare the three individual spectra (LiF1a and LiF2b from Hutchings et al. and LiF1a from the new observation) that were co-added in Figure 8, we find that Milky Way O VI is detected at >3 σ in all three individual observations, and the EWs measured from the individual spectra agree within their 1 σ uncertainties. However, O VI absorption at LMC velocities is not significantly detected in any of the individual spectra. We conclude that the current data do not show compelling evidence of O VI absorption at LMC velocities. While observations of stars in the main body of the LMC almost always show O VI absorption associated with the LMC (Howk et al. 2002), LMC X-3 is outside of the main body of the LMC (see Fig. 1), and therefore it is not necessarily surprising that the O VI is weaker in this direction. If we were to include the 2 σ absorption in the LMC velocity range, this would increase the total column density by $\approx$40% .

Over the Milky Way velocity range, we find $\log[N_{\text{O VI}}(\text{cm}^{-2})] = 14.42^{+0.07}_{-0.09}$ (1 σ uncertainties) from direct integration. Assuming a single Gaussian component for O VI, we have also used the Voigt profile fitting software of Fitzpatrick & Spitzer (1997) to measure the O VI centroid, line width, and column density, and we obtain the fit shown in Figure 8 with $v(\text{O VI}) = 55 \pm 11$ km s^{-1}, $b_v(\text{O VI}) = 81^{+18}_{-15}$ km s^{-1}, and $\log[N_{\text{O VI}}(\text{cm}^{-2})] = 14.50 \pm 0.07$. The O VI columns obtained from direct integration and profile fitting are in good agreement. The O VI column predicted from the best-fit `absline` model of the X-ray absorption lines (§ 3.1) is a factor of ~5 lower; but because of the large statistical uncertainties in the X-ray data, the discrepancy is only at the ~2 σ confidence level. Interestingly, the O VI v and b_v values are consistent with those of O VII (see Table 1 and § 3.1).

4. DISCUSSION

4.1. *Origin of the Far-UV and X-Ray Absorbers*

The centroid positions of the observed absorption lines (Table 1) may be used to determine their origin, Galactic or the LMC. Our measured centroid position of the O VII Kα line (Table 1) is consistent with the rest-frame energy and is significantly *inconsistent* with an LMC origin. The O VI line centroid differs by >10 σ from LMC velocities. Therefore, we can conclude with great confidence that the bulk of the O VI absorption detected toward LMC X-3 does not originate in the LMC. However, it remains possible that the O VI and O VII absorption occurs in separate, unrelated gas clouds, so it is important to scrutinize the disagreement between the O VII centroid and the LMC velocity. The question is whether or not any systematics may account for this disagreement. We address this question, both empirically and physically.

---

[14] The STIS observations of Sk -67 106 were obtained with the E140M echelle mode (spectral resolution = 7 km s^{-1} FWHM) and reduced as described in Tripp et al. (2001). While it might ostensibly seem more sensible to present the C II absorption observed toward Sk -67 106, since C II is detected toward LMC X-3, we prefer the O I line for two reasons: first, toward Sk -67 106, C II is badly saturated and all of the component structure evident in Fig. 8 is hidden in the black, saturated cores of the C II lines; second, and more importantly, C II at LMC velocities is badly confused by blending with C II* at Milky Way velocities (see text).

WANG ET AL.

TABLE 2
COMPARISON OF LINE CENTROID POSITIONS

Sources (OB ID)	O VII (Å)	O I (Å)	$\Delta\lambda$ (Å)
X1820–303 (98)	21.614 ± 9	23.508 ± 9	1.894 ± 13
Mrk 421 (4149)	21.603^{+9}_{-3}	23.520 ± 9	1.917^{+13}_{-9}
PKS 2155–304 (331)	21.615^{+24}_{-14}	23.514^{+21}_{-23}	1.899^{+32}_{-27}
Mean of the above.......	21.608^{+6}_{-3}	23.514 ± 6	1.906^{+9}_{-7}
LMC X-3	21.606 ± 10	23.524 ± 9	1.918 ± 13

NOTE.—The 90% confidence error bars are in units of mÅ.

Although individual lines are not resolved in the *Chandra* observations, we may determine the line centroids to an accuracy (depending on the counting statistics) comparable to the absolute photon energy scale uncertainty of the instrument. We adopt uncertainty~9 mÅ (0.19 eV) for the LETG-HRC,[15] although higher values (as high as ~50 mÅ) are also cited in documents,[16] probably resulting from evolving calibration accuracy at various stages. Table 2 compares the line centroid measurements of LMC X-3 with three other sources that have good LETG-HRC detections of both O I and O VII absorption lines. While X1820–303 is a Galactic LMXB (Futamoto et al. 2004; Yao & Wang 2005), the other two sources are AGNs (Williams et al. 2005; Yao et al. 2005, in preparation). The O VII line centroid measurements are all consistent within ~1 σ (Table 2). A maximum likelihood analysis indicates no significant intrinsic (nonstatistical) dispersion in these measurements, but the allowed 1 σ upper limit is consistent with the adopted absolute photon energy scale uncertainty. Accounting for both the statistical and systematic uncertainties, we conclude that the LMC origin of the highly ionized X-ray absorption lines detected in the LMC X-3 observations can be ruled out kinematically at ~2 σ confidence.

What is the origin of the cool oxygen absorption lines? O I and O II trace the cold and warm phases of the ISM (Field & Steigman 1971). From the EW measurements of the O I and O II Kα absorption lines, the CoG plots of Juett et al. (2004), and the Galactic ISM oxygen abundance, we estimate the equivalent hydrogen column densities of the cold and warm phases as $3.2(1.9, 5.3) \times 10^{20}$ cm^{-2} and $1.2(0.5, 2.0) \times 10^{20}$ cm^{-2}, respectively (neglecting a potential, but typically small O III contribution). These column densities, especially their lower limits, are not sensitive to the exact b_v (assumed to be 20 km s^{-1}; Reynolds 1988) and are consistent with $3.8^{+0.8}_{-0.7} \times 10^{20}$ cm^{-2} estimated from the oxygen absorption edge analysis of an *XMM-Newton* grating spectrum of LMC X-3 (Page et al. 2003). The consistent column density values are also obtained in modeling the broad band continuum observed with *BeppoSAX* (Yao et al. 2005) and *Chandra* (§ 1). The warm gas column density is in good agreement with the value expected from the so-called Reynolds layer of our Galaxy (Reynolds 1989). The cold gas is further traced by the 21 cm emission line (although with a poor spatial resolution), which gives a neutral hydrogen column density of ~4.6×10^{20} cm^{-2} in the LMC X-3 field and shows a mean velocity of ~10 km s^{-1} (Staveley-Smith et al. 2003; Dickey & Lockman 1990). There is little emission in the 100–430 km s^{-1} velocity range ($\lesssim 5 \times 10^{19}$ cm^{-2}). These values are consistent with the C II absorption seen in the UV spectrum (Fig. 8); bearing in mind that a substantial portion of the

C II feature at LMC velocities is actually due to C II* and O VI $\lambda 1037.62$ at $v = 0$ km s^{-1}, any remaining C II at $v \approx 300$ km s^{-1} could easily arise in gas with $N(H I) \ll 10^{19}$ cm^{-2}. Therefore, the cool oxygen absorption lines are also primarily Galactic.

The Galactic origin of the O I and O II absorption lines is *not* inconsistent with their velocity centroid listed in Table 1. There are considerable wavelength uncertainties in both the theoretical calculations and the laboratory measurements of the O I and O II lines. Laboratory measurements of the O I Kα transition, for example, range from 23.489 to 23.536 Å (Stolte et al. 1997), which is at least partially due to systematic uncertainties in the absolute wavelength calibration, and are probably less accurate than X-ray absorption line observations (Juett & Chakrabarty 2005). The mean centroid of the O I Kα lines listed in Table 2 is between the LETG-HRC measurement of LMC X-3 and the mean value obtained by Juett et al. (2004) from a similar analysis of *Chandra* MEG-ACIS observations of Galactic LMXBs. All these line centroid measurements agree with each other within 2 σ statistical uncertainties. It is based on these considerations that we decided to use the mean O I Kα line centroid in Table 2 as a reference for the velocity shift in Table 1. Furthermore, LMC X-3 has the Galactic coordinates of $l, b = 273°.576, -32°.082$; the conversion of our measured line-of-sight velocities into values in the local standard of rest or in the Galactic standard of rest requires a correction of -13 or -199 km s^{-1}, respectively (assuming a Galactic rotation speed of 220 km s^{-1} in the solar neighborhood and neglecting the smaller barycenter correction). Therefore, the O I and O II Kα line centroids, although with large uncertainties, are consistent with an origin in the local ISM.

We can now further constrain the origin of the O VII absorption line from its energy separation from the O I line. This relative line separation should be independent of the absolute energy scale accuracy of the observations. Table 2 shows that the separation 1918 ± 13 mÅ for the LMC X-3 is consistent with the mean value (1906^{+9}_{-7} mÅ) for the other sources and is grossly inconsistent with the value (1882 mÅ) if O VII is redshifted to the LMC X-3 velocity. Therefore, the O VII absorption line most likely does not originate in the LMC.

Of course, the above consideration of the line positions alone cannot be conclusive about the exact origin of the O VII absorption line. The systemic redshift of LMC X-3 might be compensated by a blueshift of the O VII absorber. LMC X-3 is an X-ray binary of an unseen primary compact object, which has been interpreted as a $10–15$ $M_\odot$ black hole, and a secondary star (B3 V) with an orbital period of 1.7 days (Cowley et al. 1983; Hutchings et al. 2003). The X-ray emission is apparently powered by accretion via Roche lobe overflow (Nowak et al. 2001, and references therein). An absorption line produced by a potential accretion disk and/or stellar wind should be broad and blue shifted. The expected velocity width and shift should be comparable to the escape velocity, on the order of 10^3 km s^{-1} (e.g., Yao & Wang 2005; Paerels et al. 2000), which is not consistent with our measurement of the O VII line (Table 1). Similarly, one might expect to detect a strong O VI absorption by a wind, probably in its outer regions where the ionization parameter becomes relatively small. Clearly, such a wind scenario is inconsistent with the constancy, narrowness, and rest-frame velocity of the O VI absorption detected with *FUSE*. In addition, there is no sign for any proximity effect of LMC X-3, an optical nebula or significant absorption by photoionized species (e.g., Yao & Wang 2005), indicating a lack of gas around the X-ray source. We thus tentatively conclude that the O VII as well as the O VI and O I absorption lines arise in the gas in and/or around the Galaxy.

[15] See the Chandra calibration website for CIAO 3.2 with CALDB 3.0.1; http://asc.harvard.edu/cal/.
[16] See http://cxc.harvard.edu/proposer/POG/html/MPOG.html.

4.2. *Properties of the Far-UV and X-Ray-Absorbers*

Clearly, the inference of the total column density of the X-ray-absorbing gas depends on its absolute metal abundance, which is yet to be determined observationally. We can use the dispersion measures (DMs) of pulsars observed in the vicinity of LMC X-3 to estimate the total number of free electrons along the sight line. Among the four known radio pulsars in the LMC, PSR J0502-6617 and J0529-6652 are close to the LMC X-3 sight line (Fig. 1) and have the DMs of 68.9($\pm$3) and 103.2($\pm$3) pc cm^{-3} (1 σ error bars; Crawford et al. 2001). The difference in the DMs presumably reflects the different contributions of free electrons in the LMC, because both pulsars are projected in regions with significant local Hα emission (Fig. 1). In addition, the Galactic warm H II medium is also expected to be a main (probably dominant) source of the free electrons. Therefore, we can only get an upper limit to the total hot gas column density from the DMs. The lower DM value of J0502-6617 ($l = 273°.576, b = -32°.082$), presumably least contaminated by the warm H II medium, is only slightly higher (by a factor of 1.5) than that expected from Galactic pulsar DMs, but is almost same as its highest individual value (accounting for the Galactic latitude dependence, i.e., sin b). From the comparison of our $N_{\rm O\,VI}$ estimate (§ 3.1) with the J0502-6617 DM value, we obtain an oxygen abundance as $\sim$ 19%(12%–31%)ξ^{-1} of the Galactic ISM value (§ 1), where ξ is the fraction of the electrons in the hot gas. If our estimate of the warm H II column density from the O II measurement is reasonable (§ 4.1), i.e., $1 - \xi \approx 0.57(0.24 - 0.95)$, the oxygen abundance can then be close to the ISM value or even substantially higher. Although various relevant systematics are difficult to quantify here, the lower limit to the oxygen abundance, 16% (or an O/H number ratio of 8×10^{-5}), should be quite firm. Therefore, the hot gas is unlikely to be accreted recently from the intergalactic medium (IGM).

We cany also constrain the Ne/O abundance ratio, which is used in the inference of the hot gas parameters. Published X-ray studies are all based on measurements of absorption edges, which are produced primarily by cool gas. The neutral Ne/O ratio has been determined to be 1.67 ± 0.11 and 1.10 ± 0.36 of the assumed ISM value in the sight lines of the X-ray binaries Cygnus X-1 (Schulz et al. 2002) and X-2 (Takei et al. 2002), respectively. Several X-ray binaries indicate unusually high Ne/O ratios in X-ray-absorbing gas (a factor of a few higher; Paerels et al. 2001; Juett & Chakrabarty 2005). Such high Ne/O ratios, very difficult to explain in the ISM context, are believed to arise from material local to the binaries, which typically show either coronal emission lines or burst behavior. In one occasion, the Ne/O ratio apparently varies with time (Juett & Chakrabarty 2005). With the measurements of the line absorption by the highly ionized species, it is now also possible to measure the relative metal abundances of hot gas. While we are not aware of such a measurement in publication, a joint analysis of multiple absorption lines observed in the spectra of the X-ray source 4U 1820-303 without apparent local contamination does indicate a normal Ne/O ratio of the X-ray-absorbing hot gas (Y. Yao & Q. Wang, in preparation). Similarly, if the ratio is allowed to freely vary in our `absline` fit of the LMC X-3 X-ray spectrum in § 3.1, we obtain a 95% confidence lower limit of 0.8 times the ISM value, or a Ne/O elemental number ratio of 0.14; the upper limit cannot be meaningfully constrained (Fig. 9). Therefore, the Ne/O ratio of the hot gas along the LMC X-3 sight line is consistent with a normal ISM value.

In the `absline` fit, the hot gas temperature decreases with the increase of the assumed Ne/O ratio value. But N(O VII) (or $N_{\rm H}$) hardly changes, because the ionic fraction ($\sim$1) is insensitive to
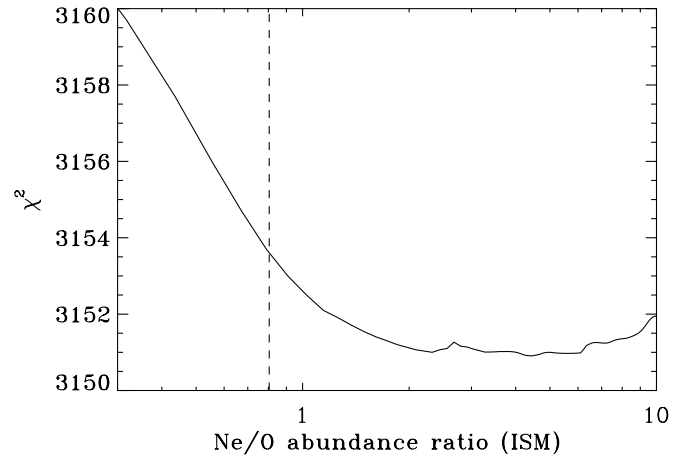

FIG. 9.—χ^2 as a function of the Ne/O ratio in a `absline` fit to the X-ray absorption lines. The vertical dashed line marks the 95% confidence lower limit to the Ne/O ratio.

the exact value of the temperature in the range of $10^{5.5}$–$10^{6.2}$ K (e.g., Yao & Wang 2005). Similarly, b_v, especially its most useful lower limit, is insensitive to the Ne/O ratio value (Fig. 7).

How are the absorbers as observed in the LMC X-3 sight line related to the general hot ISM in the Galaxy? The two AGN sight lines nearest to LMC X-3 (NGC 1705 and PKS 0558-504) do show low-velocity O VI absorption features (239 and 257 mÅ respectively, with statistical errors of about 17 mÅ; see Wakker et al. 2003), consistent with our above measurement for the LMC X-3 sight line. The inferred physical properties of the X-ray-absorbing gas along this sight line are also comparable to those along the sight lines away from the diffuse soft X-ray emission enhancement in the Galactic central region (Snowden et al. 1997). Based on nine similar detections (mainly O VII Kα and Ne IX Kα absorption lines) in the spectra of Galactic X-ray binaries and AGNs, Yao & Wang (2005) show that the hot gas column density along the sight line to LMC X-3 is consistent with a global characterization of the hot ISM in the Galaxy. Assuming a disk morphology, the vertical exponential scale height of the hot gas is $\sim$1.2 kpc. Compared with the previously measured scale heights of $\sim$2.7, 3.9, 4.4, and 5.1 kpc for O VI, N V, C IV, and Si IV, respectively (e.g., Savage et al. 1997, 2000), the hot gas appears to follow a trend from high to low ionization states away from the Galactic plane (i.e., the scale height apparently increases with the decreasing ionization potential of the species; Wang & Yao 2005). Such an ionization stratification can be understood as a result of a Galactic fountain, in which hot gas heated primarily by supernova blast waves in the Galactic disk cools off on the way to the Galactic halo (Shapiro & Field 1976; Bregman 1980).

A Galactic fountain scenario may also explain the nonthermal broadening of the far-UV- and X-ray-absorbing gas (§ 3). After the correction for the local standard of rest, the far-UV- and X-ray-absorbing hot gas along the sight line to LMC X-3 seems to have a systemic velocity close to zero, relative to the cold gas in the solar neighborhood (Table 1). Therefore, the hot gas should nearly co-rotate with the stellar (or cool gas) disk. Because of the high Galactic latitude location of LMC X-3, the line-of-sight velocity of the hot gas should hardly change through the disk with a flat rotation curve in the solar neighborhood. The expected lagging "halo" effect, as observed in diffuse cool and warm gases around nearby edge-on disk galaxies (Collins et al. 2002 and references therein), should be small on scales of the hot gas disk. Therefore, the presence of the nonthermal broadening may suggest a significant

vertical velocity gradient of the hot gas, as is expected in a Galactic fountain (Shapiro & Field 1976; Bregman 1980).

In this Galactic fountain scenario, and in the general ISM context, O VI and O VII are expected to coexist globally, although probably not in the exactly same phase. As an extreme case, we may assume that the observed O VI column all arises in the X-ray-absorbing gas and may then jointly fit the X-ray absorption lines with the *FUSE* O VI line. This fit gives $\log N_H$, b_v, $\log T$, and the Ne/O ratio of the absorbing gas as 19.5(19.3, 19.8), 74(61, 94), 5.82(5.75, 5.91), and 3.1(>1.3), respectively. The temperature obtained here represents the lowest possible limit; otherwise, the observed O VI absorption should be stronger. If only a fraction of the observed O VI absorption arises in the X-ray-absorbing gas, the temperature (Ne/O ratio) would then be greater (smaller). In general, one needs to consider the possible multiphase nature of the hot gas. O VI traces hot gas at the peak of its cooling curve and thus typically represents a very unstable transient phase, as is expected in the cooling hot gas of the Galactic fountain and/or at interfaces between hot and cool gases. Of course, the gas could in principle be in a non-CIE state, although its effect does not seem to be important for such highly ionized species as O VI and O VII in a typical ISM cooling flow (Sutherland & Dopita 1993). While a comprehensive examination of these potential complications requires data of better quality, the results from the above far-UV and X-ray joint fit should be used with extreme caution.

4.3. *Implication for Other* $cz \sim 0$ *O* VII *Absorbers*

The above discussion corroborates the conclusion that the bulk of the highly ionized gas is located near the Milky Way, most likely in a thick hot gaseous disk. The presence of this disk has strong implications for the interpretation of similar $cz \sim 0$ O VII absorbers observed in AGN spectra. Both the temperature and the line broadening of the hot gas in the LMC X-3 sight line are comparable to those of the absorbers in the AGN sight lines. In the sight line to Mrk 421 ($l = 179°.83$, $b = 65°.03$) in particular, which is also away from the Galactic central X-ray emission enhancement, the inferred vertical gas column density $N_H |\sin b| \approx 2.1 \times 10^{19}$ cm^{-2} (Yao & Wang 2005) agrees well with our measurement of 2.1(1.3, 3.4) $\times 10^{19}$ cm^{-2} in the direction of LMC X-3. But, the allowed absorbing column density beyond the LMC distance ($\lesssim 10^{19}$ cm^{-2}) may still be consistent with the recent prediction of a large-scale ($\sim 10^2$ kpc radius), very low density hot gaseous halo around the Milky Way, resulting from the accretion and cooling of the IGM (Maller & Bullock 2004). Additional contribution to O VII may also come from larger distances such as the Local Group, or even from the larger scale local filament (Williams et al. 2005; Nicastro et al. 2002). Furthermore, the hot gas properties might change from one sight line to another; a comparison between a couple of sight lines may not be considered to be conclusive. A systematic analysis of the existing data as well as sensitive new observations would be very helpful.

5. SUMMARY

We have presented our ToO *Chandra* and *FUSE* spectroscopic observations of the black hole X-ray binary LMC X-3 in its high/soft state. These observations, enhanced by archival *FUSE* data, allow us for the first time to measure both far-UV and X-ray

absorption lines along a 50 kpc sight line with little extragalactic confusion. Our main results and conclusions are as follows:

1. We have detected the absorption lines produced by the O VII Kα and Ne IX Kα transitions. A joint fit of these lines, together with the upper bounds to the O VII Kβ, and O VIII Kα lines, gives an O VII column density of $\sim 10^{16.3}$ cm^{-2} and a velocity dispersion of ~ 80 km s^{-1}. These results are insensitive to the exact Ne/O elemental number ratio, to which only a 95% confidence lower limit of 0.14 is determined. The hot gas, assumed to be in a CIE state, has a characteristic temperature in the range of $\sim 10^{6.1}$ K.

2. The X-ray-absorbing gas is likely to be primarily Galactic in origin. This conclusion is based on the consistency of both the measured absolute O VII line centroid and its relative velocity offset from the O I line, which should be predominantly Galactic. An origin of the gas in a wind from LMC X-3 may also be ruled out by the narrowness and apparent time invariance of the X-ray absorption lines.

3. The *FUSE* spectrum shows a strong ($\sim 6 \sigma$ confidence) Galactic O VI $\lambda 1031.93$ line absorption; there might be additional weak ($\sim 2 \sigma$) O VI absorption features at LMC velocities ($\sim +310$ km s^{-1}). The well resolved Galactic absorption corresponds to an O VI column density of $10^{14.5}$ cm^{-2}, which is $\sim 2 \sigma$ greater than the value expected from the X-ray absorption line modeling. This discrepancy may indicate a multiphase state of the absorbing gas.

4. We speculate that the highly ionized absorbing gas represents a supernova-driven Galactic fountain, which globally resembles a thick gaseous disk with decreasing ionization away from the Galactic plane. In particular, this Galactic fountain scenario naturally explains the significant nonthermal velocity broadening inferred from the direct O VI line width measurement and from the relative strengths of the X-ray absorption lines. We further trace the warm H II gas along the LMC X-3 sight line with our detected O II Kα line. From the X-ray absorption measurements and the Galactic (pulsar) dispersion measure in the LMC X-3 vicinity, we estimate the oxygen abundance of the X-ray absorbing gas to be $\gtrsim 16\%$ of the Galactic ISM value. Therefore, the X-ray-absorbing gas is metal rich.

5. The X-ray absorption lines along the LMC X-3 sight line have properties similar to those of other $cz \sim 0$ highly ionized absorbers observed in the spectra of Galactic X-ray binaries and extragalactic AGNs (Yao & Wang 2005). While there is still room for a significant presence of very low-density diffuse hot gas on scales greater than 50 kpc (e.g., the Local Group), any such extragalactic studies of highly ionized species at $z \sim 0$ must take into account the Galactic hot ISM component.

REFERENCES

Bregman, J. N. 1980, ApJ, 236, 577
Cen, R., & Ostriker, J. P. 1999, ApJ, 514, 1
Collins, J. A., Benjamin, R. A., & Rand, R. J. 2002, ApJ, 578, 98
Collins, J. A., Shull, J. M., & Giroux, M. L. 2005, ApJ, 623, 196
Cowley, A. P., et al. 1983, ApJ, 272, 118
———. 1991, ApJ, 381, 526

Crawford, F., et al. 2001, ApJ, 553, 367
Danforth, C. W., Howk, J. C., Fullerton, A. W., Blair, W. P., & Sembach, K. R. 2002, ApJS, 139, 81
Davé, R., et al. 2001, ApJ, 552, 473
Dickey, J. M., & Lockman, F. J. 1990, ARA&A, 28, 215
Fang, T., Bryan, G. L., & Canizares, C. R. 2002a, ApJ, 564, 604
Fang, T., Sembach, K. R., & Canizares, C. R. 2003, ApJ, 586, 49
Fang, T., et al. 2002b, ApJ, 572, 127
Field, G. B., & Steigman, G. 1971, ApJ, 166, 59
Finkbeiner, D. P. 2003, ApJS, 146, 407
Fitzpatrick, E. L., & Spitzer, L. 1997, ApJ, 475, 623
Fukugita, M., Hogan, C. J. & Peebles, J. P. E. 1998, ApJ, 503, 518
Futamoto, K., et al. 2004, ApJ, 605, 793
Grevesse, N., & Sauval, A. J. 1998, Space Sci. Rev., 85, 161
Howk, J. C., Sembach, K. R., Savage, B. D., Massa, D., Friedman, S. D., & Fullerton, A. 2002, ApJ, 569, 214
Hutchings, J. B., Winter, K., Cowley, A. P., Schmidtke, P. C., & Crampton, D. 2003, AJ, 126, 2368
Juett, A. M., & Chakrabarty, D. 2005, ApJ, 627, 926
Juett, A. M., Schulz, N. S., & Chakrabarty, D. 2004, ApJ, 612, 308
Kawatsura, K., et al. 2002, J. Phys. B, 35, 4147
Kirkman, D., & Tytler, D. 1997, ApJ, 489, L123
Maller, A. H., & Bullock, J. S. 2004, MNRAS, 355, 694
Mathur, S., Weinberg, D. H., & Chen, X. 2003, ApJ, 582, 82
McKernan, B., Yaqoob, T., & Reynolds, C. S. 2004, ApJ, 617, 232
Moos, H. W., et al. 2000, ApJ, 538, L1
———. 2002, ApJS, 140, 3
Nicastro, F., et al. 2002, ApJ, 573, 157
———. 2005, ApJ, 629, 700
Nowak, M. A., et al. 2001, MNRAS, 320, 316
Paerels, F., et al. 2000, ApJ, 533, L135
———. 2001, ApJ, 546, 338
Page, M. J., et al. 2003, MNRAS, 345, 639
Rasmussen, A., Kahn, S. M., & Paerels, F. 2003, in The IGM/Galaxy Connection: The Distribution of Baryons at $z = 0$, ed. J. L. Rosenberg & M. E. Putman (Dordrecht: Kluwer), 109

Reimers, D., Baade, R., Hagen, H.-J, & Lopez, S. 2001, A&A, 374, 871
Reynolds, R. J. 1988, ApJ, 333, 341
———. 1989, ApJ, 339, L29
Savage, B. D., Lehner, N., Wakker, B. P., Sembach, K. R., & Tripp, T. M. 2005a, ApJ, 626, 776
Savage, B. D., Wakker, B. P., Fox, A. J., & Sembach, K. R. 2005b, ApJ, 619, 863
Savage, B. D., et al. 1997, AJ, 113, 2158
———. 2000, ApJ, 538, L27
Schulz, N. S., et al. 2002, ApJ, 565, 1141
Sembach, K. R., & Savage, B. D. 1992, ApJS, 83, 147
Sembach, K. R., Tripp, T. M., Savage, B. D., & Richter, P. 2004, ApJS, 155, 351
Shapiro, P. R., & Field, G. B. 1976, ApJ, 205, 762
Simcoe, R. A., Sargent, W. L. W., & Rauch, M. 2002, ApJ, 578, 737
Snowden, S. L., et al. 1997, ApJ, 485, 125
Staveley-Smith, L., Kim, S., Calabretta, M. R., Haynes, R. F. & Kesteven, M. J. 2003, MNRAS, 339, 87
Stolte, W. C., et al. 1997, J. Phys. B, 30, 4489
Sutherland, R. S. & Dopita, M. A. 1993, ApJS, 88, 253
Takei, Y., et al. 2002, ApJ, 581, 307
Tripp, T. M., Giroux, M. L., Stocke, J. T., Tumlinson, J., & Oegerle, W. R. 2001, ApJ, 563, 724
Tripp, T. M., & Savage, B. D. 2000, ApJ, 542, 42
Tripp, T. M., Savage, B. D., & Jenkins, E. B. 2000, ApJ, 534, L1
Wakker, B. P., et al. 2003, ApJS, 146, 1
Wang, Q. D., & Yao, Y. 2005, in AIP Conf. Ser. 774, X-ray Diagnostics for Astrophysical Plasmas, ed. Randall K. Smith (Greenbelt: Goddard Space Flight Center), 191
Williams, R. J., et al. 2005, ApJ, 631, 856
Wilms, J., Allen, A., & McCray, R. 2000, ApJ, 542, 914
Yao, Y., & Wang, Q. D. 2005, ApJ, 624, 751
Yao, Y., Wang, Q. D., & Zhang, S. N. 2005, MNRAS, 362, 229